NJC

ROYAL SOCIETY OF CHEMISTRY

PAPER

View Article Online
View Journal | View Issue

Cite this: *New J. Chem.*, 2022, **46**, 11946

A new diformyl phenol based chemosensor selectively detects Zn^{2+} and Co^{2+} in the nanomolar range in 100% aqueous medium and HCT live cells†

Barnali Naskar,[ab] Chitrangada Das Mukhopadhyay[c] and Sanchita Goswami *[a]

In this manuscript, we present a chemosensor, 4-methyl-2,6-bis-[(2-pyridin-2-yl-ethylimino)-methyl]-phenol (**Hmpye**), for selective detection of Zn^{2+} and Co^{2+} in 100% aqueous medium. The active component of the sensor is the Schiff base condensation product between 4-methyl-2,6-diformyl-phenol and 2,2-pyridyl ethylamine and the resultant moiety is ESIPT (excited-state intramolecular proton transfer) active *via* imine nitrogen and phenolic OH. The absorption and emission spectral investigations have been carried out extensively for the sensing system which showed that **Hmpye** is able to sense Zn^{2+} by fluorescence turn-on and Co^{2+} by fluorescence turn-off. Apart from Job's plot and ESI-MS studies, the single crystal X-ray diffraction study has been utilized to ascertain the 1 : 2 ratio of the sensor : Zn^{2+} ensemble. The detection limits for Zn^{2+} and Co^{2+} are 4.683×10^{-9} (M) and 7.591×10^{-9} (M), respectively. The sensing capability of **Hmpye** has also been checked in HCT live cells. The potential of the work has been demonstrated by the fact that nanomolar detection of Zn^{2+} and Co^{2+} from 100% aqueous solution can be achieved by a single probe which is scarce in the literature.

Received 25th March 2022,
Accepted 23rd May 2022

DOI: 10.1039/d2nj01478e

rsc.li/njc

1. Introduction

Schiff base chemosensors represent an important niche in the field of sensing.[1] Among different analytes, Zn^{2+} and Co^{2+} play critical roles in various biological processes, whereas their excess accumulation or deficiency could lead to serious health conditions in human beings. Zn^{2+} is the most abundant essential trace element and participates in a wide range of cellular functions of the body, such as acting as a cofactor of carbonic anhydrase and zinc-finger proteins (ZNFs), DNA synthesis, RNA transcription, regulation of metalloenzymes, neurophysiology, and apoptosis.[2] Apart from that, our brain registers the highest concentration of Zn^{2+} (150–300 nM) and thus it plays a significant role in synaptic transmission.[3] Natural and anthropogenic sources like volcanic eruptions and mining are the ways by which zinc is released in the environment. Consumption of vegetables and fruits grown in zinc contaminated areas poses a threat of overaccumulation of zinc in the human body.[4a,b] A minute imbalance of Zn^{2+} in the human body can lead to serious diseases like diabetes, neurodegenerative disorders (Alzheimer's disease), and certain types of cancer.[4c–f]

The available analytical techniques for Zn^{2+} determination include atomic absorption spectrometry,[5] inductively coupled plasma mass spectrometry (ICPMS),[6] and inductively coupled plasma atomic emission spectrometry (ICPAES),[7] but they are not operative *in situ* and in real time, especially in the biological systems of live cells.[8]

On the other hand, Co^{2+} is a naturally occurring element in the Earth's crust, water, animals and plants and it is present in almost all cellular organisms, such as the liver, bones and kidneys, and takes part in the signaling process.[9] Co^{2+} is the chief component of vitamin B12 and other cobalamines and plays an important role in the metabolism of iron and synthesis of hemoglobin.[10] The excess accumulation/deficiency of cobalt causes delayed growth, anemia, loss of appetite, decreased lactation, heart disease, lung damage, asthma, pneumonia and thyroid enlargement.[11,14–16] Co^{2+} exposure mainly originates from hard metal, diamond polishing, porcelain, chemical, and pharmaceutical industries.[12,13]

Instrumental methods for sensing Co^{2+} include[17] inductively coupled plasma atomic emission spectrometry (ICPAES),[18] atomic absorption spectroscopy,[19] and electrochemical methods.[20]

[a] *Department of Chemistry, University of Calcutta, 92, A. P. C. Road, Kolkata 700009, India. E-mail: sgchem@caluniv.ac.in*
[b] *Department of Chemistry, Lalbaba College, University of Calcutta, Howrah 711202, India*
[c] *Centre for Healthcare Science & Technology, Indian Institute of Engineering Science and Technology, Shibpur, Howrah 711103, India*

† Electronic supplementary information (ESI) available: NMR spectra, FT-IR spectra, ESI-MS spectra, crystallographic data, photophysical characterization, and cell viability. CCDC 2161072. For ESI and crystallographic data in CIF or other electronic format see DOI: https://doi.org/10.1039/d2nj01478e

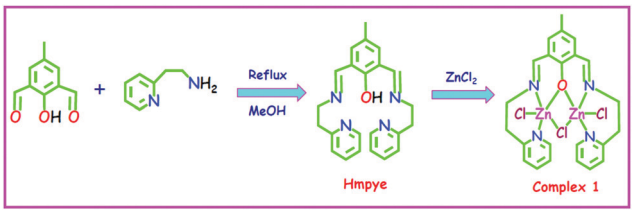

Scheme 1 Scheme for the synthesis of the ligand (**Hmpye**) in complex **1**.

However, these methods require sophisticated equipment, tedious sample preparation procedures, large sample volumes and trained operators which are costly and not suitable for on-site experimentation. In comparison, colorimetric/fluorimetric chemosensors provide high selectivity and sensitivity of analyte sensing, fast response, and real-time measurement facility and require less expensive instrumentation.[21,22]

In view of the above considerations, precise determination of Zn^{2+} and Co^{2+} is highly important for the mankind and chemosensors have significantly contributed in this area. In this paper we have designed a diformyl phenol based chemosensor, 4-methyl-2,6-bis-[(2-pyridin-2-yl-ethylimino)-methyl]-phenol (**Hmpye**), produced from 4-methyl-2,6-diformylphenol and 2,2-pyridyl ethylamine (**Hmpye** sketched in Scheme 1) for selective detection of Zn^{2+} and Co^{2+} in 100% aqueous solution. We have made a comparison of recently reported chemosensors that can sense Zn^{2+}+ Co^{2+} as well as Zn^{2+}/Co^{2+} in the literature[1d,e,23] (Table S5, ESI†) which revealed only two chemosensors for simultaneous detection of Zn^{2+} and Co^{2+} from 100% aqueous solution in the micromolar range. Interestingly, our reported system can sense Zn^{2+} and Co^{2+} from 100% aqueous solution in the nanomolar range.

2. Experimental section

2.1. Materials and physical methods

2,2-Pyridyl ethylamine, $ZnCl_2$, $CoCl_2$ and HEPES buffer were purchased from Sigma-Aldrich. The buffer was prepared using triple distilled water. The solvents used for spectroscopic studies and for the syntheses were purchased from commercial sources and used as received. Powder X-ray diffraction (PXRD) patterns were acquired using a PANalytical X'Pert PRO diffractometer (The Netherlands) operated at 40 kV and 30 mA with graphite monochromatized Mo Kα radiation of wavelength = 0.71073 Å and a nickel filter. Elemental analyses for C, H and N were performed on a PerkinElmer 2400 II analyzer. The FT-IR spectra were recorded from KBr pellets in the range of 400–4000 cm^{-1} on a PerkinElmer Spectrum 100 spectrometer. ^1H and ^{13}C NMR spectra were recorded in d_6-DMSO with TMS as the internal standard on a Bruker AV 300 Supercon Digital NMR system. The ESI-MS spectra were recorded on a Qtof Micro YA263 mass spectrometer. A Systronics digital pH meter (model 335) was used to measure the pH of the solution and the adjustment of pH was done using either 50 mM HCl or NaOH solution. The absorption and emission spectra were recorded on a Hitachi UV-Vis U-3501 spectrophotometer and a PerkinElmer LS55 fluorimeter, respectively. Time-resolved fluorescence lifetime measurements were performed with a Horiba Jobin Yvon Fluorocube-01-NL time-correlated single photon counting (TCSPC) set-up employing a picosecond delta diode (DD-375L) operating at λ_{ex} = 375 nm and a repetition rate of 1 MHz as the excitation source. The overall temporal and spectral resolution of the instrument was ~60 ps. The average fluorescence lifetimes (τ_{avg}) were calculated from the decay times and pre-exponential factors using the following equation:

$$\tau_{avg} = \frac{\sum \alpha_i \tau_i^2}{\sum \alpha_i \tau_i}$$

where α_i is the pre-exponential factor corresponding to the ith decay time constant, τ_i.

For the titration experiment, we used the cations, *viz.* [Li^+, Na^+, K^+, Ca^{2+}, Mg^{2+}, Mn^{2+}, Ba^{2+}, Cu^{2+}, Ni^{2+}, Co^{2+}, Fe^{2+}, Fe^{3+}, Zn^{2+}, Cd^{2+}, Hg^{2+}, Pb^{2+}, Sr^{2+} and Cr^{3+}], as their chloride salts and the nitrate salt of Al^{3+} was used. The fluorescence quantum yield (Φ) was determined using the quinine sulphate (Φ_R) reference using the following equation:

$$\Phi_S = \Phi_R \frac{A_S}{A_R} \times \frac{Abs_R}{Abs_S} \times \frac{\eta_S^2}{\eta_R^2}$$

where the A terms denote the integrated area under the fluorescence curve, Abs denotes the absorbance, η is the refractive index of the medium and Φ is the fluorescence quantum yield. Subscripts S and R denote the respective parameters for the studied sample and reference, respectively.

2.2. Synthesis and characterisation

Synthesis of the ligand 4-methyl-2,6-bis-[(2-pyridin-2-yl-ethylimino)-methyl]-phenol (Hmpye). The synthesis of 4-methyl-2,6-diformylphenol (2-hydroxy-5-methyl-benzene-1,3-dicarbaldehyde) was carried out by modifying a previously published literature procedure.[24a] 4-Methyl-2,6-diformylphenol (0.328 g, 2 mmol) was dissolved in methanol, followed by the dropwise addition of methanol solution of 2,2-pyridyl ethylamine (0.488 g, 4 mmol) with constant stirring for 30 min. The resulting reaction mixture was refluxed for 6 h. The solution was then cooled to room temperature, concentrated on a rota-evaporator to get (93%) an oily yellow liquid compound which was recrystallized from methanol for purification and used throughout the experiment and characterization. Anal. calcd. for $C_{23}H_{24}N_4O$: C, 74.17; H, 6.49; N, 15.04; found: C, 74.16; H, 6.48; N, 15.05; ^1H NMR (300 MHz, DMSO-d_6) δ_H: 13.67 (1H), 8.43 (s, 2H), 7.62–7.56 (m, 2H), 7.35 (s, 2H), 7.18 (d, J = 7.8 Hz, 2H), 7.14–7.09 (m, 2H), 3.86 (t, J = 6.9 Hz, 4H), 2.98 (t, J = 7.1 Hz, 4H), 2.11 (s, 3H); ^{13}C NMR (300 MHz, DMSO-d_6) δ_C: 160.6, 159.1, 158.7, 148.6, 135.9, 131.8, 125.9, 122.9, 121.0, 120.3, 58.3, 38.2, 19.4 (Fig. S1, ESI†); selected FT-IR data (KBr, cm^{-1}) $\nu_{(OH)}$ = 3434.29 cm^{-1}, $\nu_{(C=N)}$ = 1603.98 cm^{-1} (Fig. S2, ESI†). ESI-MS m/z, ion: 373.1802, [**Hmpye** + H]$^+$, $C_{23}H_{25}N_4O$ (Fig. S3, ESI†).

General procedure for the syntheses of complexes 1 and 2. The two metal complexes were synthesized using the following general procedure: **Hmpye** (0.372 g, 1.0 mmol) was dissolved in methanol (10 mL). MX_2 (M = Zn and Co, X = Cl) was added to this solution.

The reaction mixture was refluxed for 4 h to afford a clear solution and then the solution was filtered off. The filtrate was kept aside undisturbed for slow evaporation. After about two days, single crystals, suitable for X-ray diffraction analysis (except for M = Co and X = Cl), were isolated. Specific details of each reaction and the characterization data for these complexes are given below.

$[Zn_2(mpye)(Cl)_3]$ (1). Quantities: **Hmpye** (0.372 g, 1.0 mmol), $ZnCl_2$ (0.272 g, 2 mmol). Yield: 85%. Anal. calcd for $C_{23}H_{23}N_4OZn_2Cl_3$ (608.59): C, 45.39; H, 3.81; N, 9.21; found: C, 45.38; H, 3.82; N, 9.20. FT-IR (KBr, cm^{-1}): $\nu_{(OH)}$ = 3434.18 cm^{-1}, $\nu_{(C=N)}$ = 1648.35 cm^{-1} (Fig. S2, ESI†). ESI-MS *m*/*z*, ion: 568.9149, [(**mpye**) + $(Zn)_2$ + $(Cl)_2]^+$, $C_{23}H_{23}N_4OZn_2Cl_2$; 586.9397 [(**mpye**) + $(Zn)_2$ + $(Cl)_2$ + $H_2O]^+$, $C_{23}H_{25}N_4O_2Zn_2Cl_2$ (Fig. S3, ESI†).

$[Co_2(mpye)(Cl)_3]$ (2). Quantities: **Hmpye** (0.372 g, 1.0 mmol), $CoCl_2$ (0.259 g, 2 mmol). Yield: 92%. Anal. calcd for $C_{23}H_{23}N_4OCo_2Cl_3$ (595.68): C, 46.37; H, 3.89; N, 9.41; found: C, 46.38; H, 3.88; N, 9.40. FT−IR (KBr, cm^{-1}): $\nu_{(OH)}$ = 3434.12 cm^{-1}, $\nu_{(C=N)}$ = 1656.59 cm^{-1} (Fig. S2, ESI†). ESI-MS *m*/*z*, ion: 594.1738, [(**mpye**) + $(Co)_2$ + $(Cl)_3$+ H]$^+$, $C_{23}H_{24}N_4OCo_2Cl_3$ (Fig. S3, ESI†).

2.3. Cell study of Hmpye

Materials and methods. The frozen human colorectal carcinoma cell line **HCT116** and HeLa cells were obtained from NCCS, Pune, India and maintained in Dulbecco's modified Eagle's medium (DMEM, Sigma Chemical Co., St. Louis, MO, USA) supplemented with 10% fetal bovine serum (Invitrogen), penicillin (100 μg mL^{-1}), and streptomycin (100 μg mL^{-1}). The cells were initially propagated in a 25 cm^2 tissue culture flask under an atmosphere of 5% CO_2 and 95% air at 37 °C with the humidification till 70–80% confluency.

Fluorescence imaging studies. For fluorescence imaging studies, **HCT116** at 1 × 10^{-5} cells in 150 μL medium were seeded on a sterile 12 mm diameter poly-L-lysine coated coverslip, kept in a sterile 35 mm covered Petri dish and incubated at 37 °C in a CO_2 incubator for 24–30 h. The next day, cells were washed three times with phosphate buffered saline (pH 7.4), fixed using 4% paraformaldehyde in PBS (pH 7.4) for 10 minutes at room temperature and again washed with PBS, followed by permeabilization using 0.1% saponin for 10 minutes. Then the cells were incubated with 2.0 × 10^{-4} M of $Zn(NO_3)_2{\cdot}6H_2O$ for 30 min at 37 °C for 1 h in a CO_2 incubator. Cells were washed using PBS buffer (pH 7.4) gently 3 times to get rid of the extra metal salt and observed under a spinning disk confocal microscope (Fig. 6, panel a–c) upon excitation using a 340 nm monochromatic laser beam and the collected range of emission wavelength was between 420 nm and 505 nm. Images were captured using an EMCCD camera with a 40× objective lens. In a similar set of experiments cells were treated with $Zn(NO_3)_2{\cdot}6H_2O$, followed by incubation in 1.0 × 10^{-4} M **Hmpye** dissolved in 100 μL HEPES buffer at 37 °C for 1 h in a CO_2 incubator. Cells were washed to remove the extra salt and probe, counterstained with DAPI (1 μg mL^{-1}) and mounted on a slide to capture images in a similar way. In a 3rd set of experiments the cells were treated first with 2.0 × 10^{-4} M of $Zn(NO_3)_2{\cdot}6H_2O$ for 30 min, then **Hmpye** was dissolved in 100 μL HEPES buffer at 37 °C for 1 h, followed by 2.0 × 10^{-4} M of $Co(NO_3)_2{\cdot}6H_2O$ for 30 min. After each treatment the cells were washed gently with PBS. Images were captured (Fig. 7(a)–(c)) using an EMCCD camera upon excitation using a 340 nm monochromatic laser beam and the collected range of emission wavelength was between 460 nm and 520 nm. Before fluorescence imaging all the solutions were aspirated out and mounted on slides in a mounting medium containing DAPI (1 μg mL^{-1}) and stored in the dark before acquiring the microscopic images.

Cytotoxicity assay. The cytotoxic effects of the probe (**Hmpye**), $Zn(NO_3)_2{\cdot}6H_2O$, $Co(NO_3)_2{\cdot}6H_2O$, and the probe–Zn^{2+}/Co^{2+} complex were determined by the MTT assay following the manufacturer's instructions (MTT 2003, Sigma-Aldrich, MO). Briefly HCT 116 cells were cultured into 96-well plates (approximately 10^4 cells per well) for 24 h. The next day the medium was removed and various concentrations of **Hmpye**, Zn^{2+}/Co^{2+} salts and the **Hmpye**–Zn^{2+}/Co^{2+} complex (0, 20, 30, 50, 75, and 100 μM) were added to the cells and incubated for 24 h. Control samples with no cells and cells in the DMEM nutrient medium without any treatment were also included in the study. Following incubation, the growth medium was removed and MTT solution was added. The plate was incubated for 3–4 h at 37 °C. Subsequently, the supernatant was removed, the insoluble colored formazan product was solubilized in DMSO, and its absorbance was measured using a microtiter plate reader (PerkinElmer) at 570 nm. The assay was performed in triplicate for each concentration of the probe, Zn^{2+}/Co^{2+} salt and probe–Zn^{2+}/Co^{2+} complex. The OD value of wells containing only DMEM was subtracted from all readings to get rid of the background influence. Data analysis and calculation of standard deviation was performed with Microsoft Excel 2010 (Microsoft Corporation).

2.4. Single-crystal X-ray crystallography

The single-crystal X-ray diffraction study of complex **1** was performed on a Nonius APEX-II diffractometer with a CCD-area detector at 296 K using graphite-monochromated Mo Kα radiation (λ = 0.71073 Å). The structure was solved by direct methods and successive Fourier difference syntheses, and refined by the full-matrix least-squares method on F^2 with the SHELXL-97 program.[25] Multi-scan absorption corrections were applied using the SADABS program. The locations of the metal atom and O, N, and C atoms were subsequently determined from the difference Fourier maps. All non-hydrogen atoms were refined with anisotropic displacement parameters. Most of the hydrogen atoms were placed in the idealized positions and refined as riding atoms with individual isotropic displacement parameters. The crystal parameters and the results of data collection and refinement are summarized in Table S1 (ESI†). CCDC 2161072 contains the supplementary crystallographic data for this paper.† The crystallographic figures presented in this manuscript were generated using Diamond 3.0 software.[26] Crystallographic details are available in CIF format.

3. Results and discussion

3.1. Syntheses and general characterization

The synthesis of **Hmpye** involved an one-step simple Schiff-base condensation reaction of 4-methyl-2,6-diformylphenol with

2,2-pyridyl ethylamine in a 1 : 2 molar ratio in methanol solution and characterized by ^{1}H and ^{13}C NMR spectroscopy, FT-IR spectroscopy, ESI-MS and elemental analysis (Fig. S1–S3, ESI†). The **Hmpye** ligand possesses five coordination sites, including two imino nitrogen atoms, one phenolic oxygen atom, and two pyridine nitrogen atoms (Scheme 1). By modifying the previously published literature procedure, **Hmpye** was allowed to react with $ZnCl_2$ and $CoCl_2$ in a 1 : 2 stoichiometric ratio in the presence of methanol solution, which afforded dinuclear complexes $[Zn_2(mpye)(Cl)_3]$ (**1**) and $[Co_2(mpye)(Cl)_3]$ (**2**).[24b] The electrospray ionization mass spectrometry (ESI-MS) spectra of complexes **1** and **2** reveal that they retain their molecular integrity in solution, as indicated by the presence of molecular ion peaks. The experimental powder XRD patterns of the bulk crystalline material are in good agreement with the simulated XRD patterns of single crystal X-ray diffraction, confirming the purity of the bulk samples (Fig. S4, ESI†). The molecular structure of complex **1** was confirmed by single-crystal X-ray crystallography studies.

3.2. Structure description of the complex $[Zn_2(mpye)(Cl)_3]$ (1)

Complex **1** was crystallized in the orthorhombic crystal lattice system in the *Pbcn* space group with $Z = 4$ (Table S1, ESI†). The asymmetric unit contains two zinc (Zn1 and Zn2) centers and one **Hmpye** ligand (Fig. 1). The coordination environment of each zinc center around Zn1 and Zn2 is made up of one phenolato oxygen atom O1 for Zn1 and Zn2, one imino nitrogen (N2 for Zn1 and N1 for Zn2), one pyridine nitrogen (N3 for Zn1 and N4 for Zn2) and two chlorine atoms (Cl1 and Cl3 for Zn1, and Cl2 and Cl3 for Zn2), displaying a five coordinated spherical square pyramidal geometry for Zn1 and a trigonal bipyramidal geometry for Zn2 (Scheme 2 and Scheme S1, ESI†). The zinc centers in complex **1** are intermediate between square pyramidal and trigonal bipyramidal geometries with τ values of 0.545 and 0.204 for Zn1 and Zn2, respectively.[27] Therefore, we have performed a continuous shape measurement analysis considering both five-coordinated zinc centers and the outcome

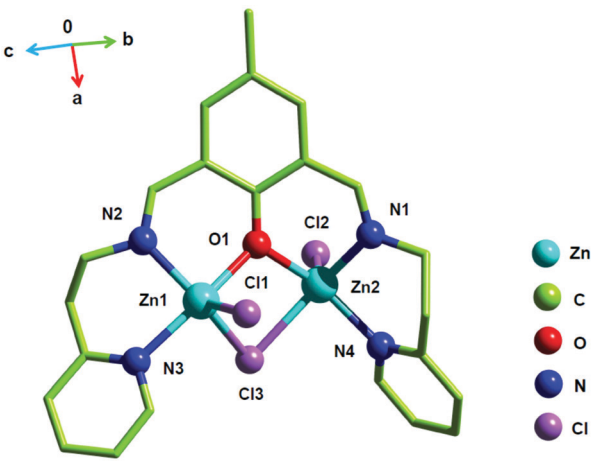

Fig. 1 Solid state structure of complex **1** with a partial atom numbering scheme.

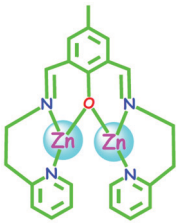

$\eta^2:\eta^2:\eta^2:\mu_2$

Scheme 2 Coordination and bridging modes of the ligand (**Hmpye**) in complex **1**.

indicates a five-coordinated square pyramidal and a trigonal bipyramidal geometry with minimum deviations of 0.805 for Zn(1) and 1.725 for Zn(2) (out of the range 0.1–3, CShM value; Table S3, ESI†). The bond lengths of the Zn1 centre are 2.092(3) Å for Zn(1)–O(1), 2.057(5) Å for Zn(1)–N(2), and 2.169(5) Å for Zn(1)–N(3) and those for the Zn2 centre are 2.032(4) Å for Zn(2)–O(1), 2.078(5) Å for Zn(2)–N(1), and 2.110(5) Å for Zn(2)–N(4) (Table S2, ESI†). The separation of intramolecular Zn1···Zn2 is 3.388 Å.

3.3. Absorption and fluorescence spectroscopy studies of Hmpye

The absorption spectral properties of **Hmpye** were studied in HEPES buffer (pH = 7.4) solution which exhibit strong absorbance bands at 450 nm and 340 nm. Upon addition of Zn^{2+}, there is a decrease in absorbance intensity at 450 nm and 340 nm with the appearance of a new absorption band at 390 nm (Fig. S5, ESI†). Furthermore, upon incremental addition of Co^{2+} to a solution of **Hmpye** the absorption peak at 450 nm decreases along with a new absorption band at 392 nm (Fig. S6, ESI†).

To ascertain the stoichiometry of the **Hmpye–analyte** entity, Job's plots for the binding activity between **Hmpye** and Zn^{2+} and Co^{2+} were analyzed, and the results exhibited a 1 : 2 stoichiometry from the absorbance titration profile at 390 nm (for Zn^{2+}) and at 450 nm (for Co^{2+}) (Fig. S7 and S8, ESI†). The stoichiometry of both the complexes was also well corroborated by ESI-MS spectra where the molecular ion peak at m/z = 568.9149, $[(\mathbf{mpye}) + (Zn)_2 + (Cl)_2]^+$, $C_{23}H_{23}N_4OZn_2Cl_2$; 586.9397 $[(\mathbf{mpye}) + (Zn)_2 + (Cl)_2 + H_2O]^+$, $C_{23}H_{25}N_4O_2Zn_2Cl_2$ for complex **1** (Fig. S3, ESI†). The mass spectrum of complex **2** exhibited a prominent peak at m/z, ion: 594.1738 amu assignable to $[(\mathbf{mpye}) + (Co)_2 + (Cl)_3 + H]^+$, $C_{23}H_{24}N_4OCo_2Cl_3$ (Fig. S3, ESI†).

To gain an insight into the fluorescence outcome of **Hmpye** (λ_{ex} = 340 nm, λ_{em} = 503 nm) toward metal ions, the emission changes were measured in the presence of various metal ions in HEPES buffer (pH = 7.4) solution. The fluorescence titrations of **Hmpye** were carried out by gradual addition of various concentrations (0–2.0 equiv.) of Zn^{2+} (Fig. 2) and it manifested a remarkable enhancement (Φ = 0.325 to Φ = 0.610) in the fluorescence at 461 nm, whereas the incremental addition of 2.0 equiv. of Co^{2+} (Fig. 3) to the solution of **Hmpye** induces 13-fold quenching of the fluorescence intensity at 503 nm

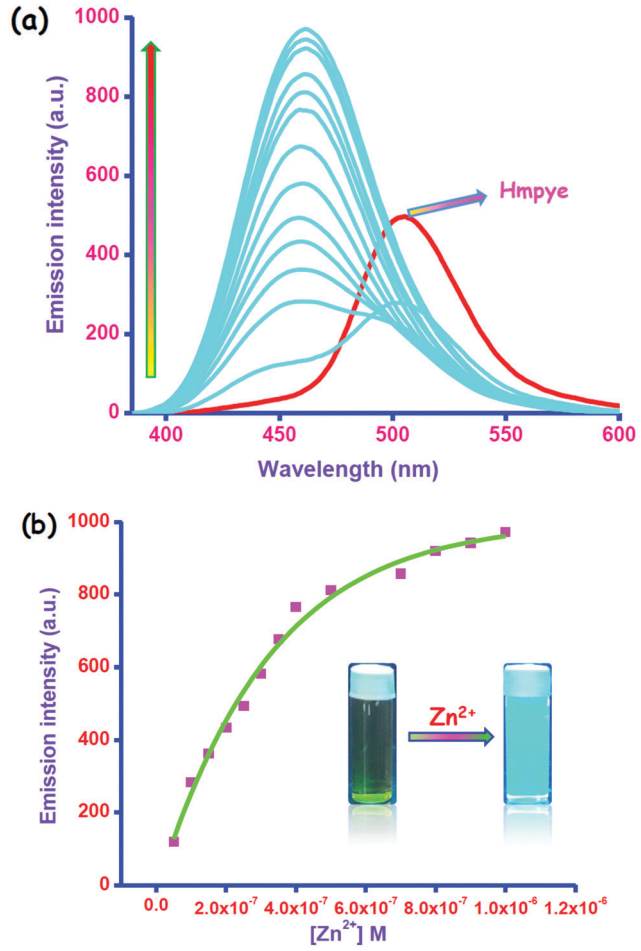

Fig. 2 (a) Emission spectra of **Hmpye** (5×10^{-7} M) in the presence of increasing amounts of $[Zn^{2+}]$ (0, 0.5, 1, 1.5, 2, 2.5, 3, 4, 5, 6, 7, 8, 9 and 10 ($\times 10^{-7}$) M in HEPES buffer (pH = 7.4) solution (λ_{ex} = 340 nm, λ_{em} = 461 nm). (b) Fluorescence emission intensity of **Hmpye** at 461 nm as a function of $[Zn^{2+}]$.

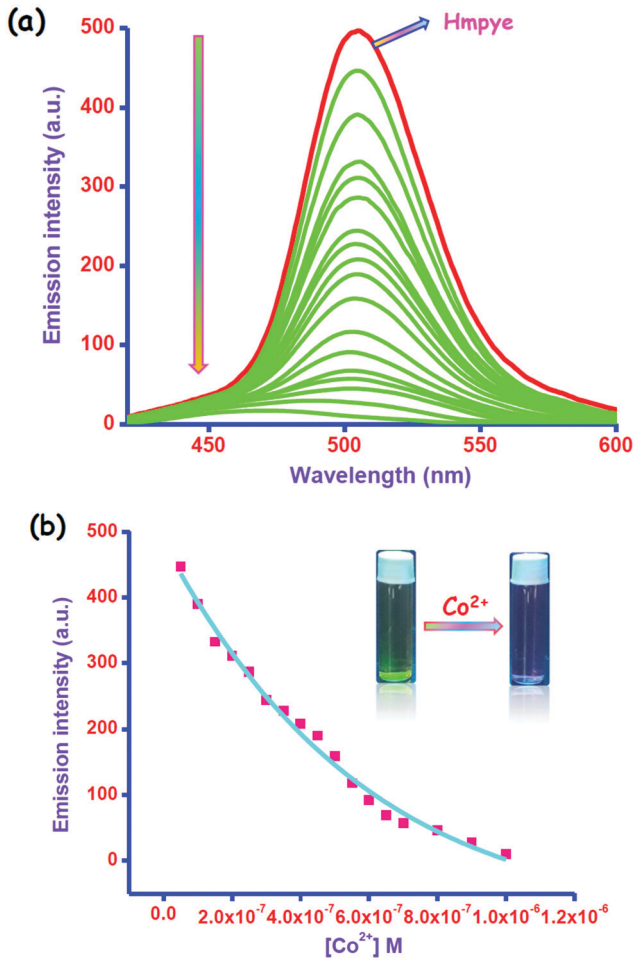

Fig. 3 (a) Emission spectra of **Hmpye** (5×10^{-7} M) in the presence of increasing amounts of $[Co^{2+}]$ (0, 0.5, 1, 1.5, 2, 2.5, 3, 3.5, 4, 4.5, 5, 5.5, 6, 6.5, 7, 8, 9 and 10 ($\times 10^{-7}$) M in HEPES buffer (pH = 7.4) solution (λ_{ex} = 340 nm, λ_{em} = 503 nm). (b) Fluorescence emission intensity of **Hmpye** at 503 nm as a function of $[Co^{2+}]$.

(Φ = 0.025). By contrast, upon addition of other metal ions such as Li^+, Na^+, K^+, Ca^{2+}, Mg^{2+}, Mn^{2+}, Ba^{2+}, Cu^{2+}, Ni^{2+}, Fe^{2+}, Fe^{3+}, Cd^{2+}, Hg^{2+}, Pb^{2+}, Sr^{2+}, Al^{3+} and Cr^{3+}, either no or a slight increase or decrease in intensity was observed (Fig. 4 and 5). These results confirmed that **Hmpye** is a highly specific sensor for Zn^{2+} and Co^{2+} with an "ON–OFF" optical function.

To investigate the practical application of **Hmpye** for Zn^{2+}/Co^{2+} detection, the effect of competitive metal ions was investigated by adding Zn^{2+}/Co^{2+} to the **Hmpye** solution in the presence of the metal ions Li^+, Na^+, K^+, Ca^{2+}, Mg^{2+}, Mn^{2+}, Ba^{2+}, Cu^{2+}, Ni^{2+}, Fe^{2+}, Fe^{3+}, Cd^{2+}, Hg^{2+}, Pb^{2+}, Sr^{2+}, Al^{3+} and Cr^{3+}, as shown in Fig. 4 and 5, which reaffirms the selective detection of Zn^{2+} and Co^{2+}. From the fluorescence titration data, the detection limits (LODs) were also calculated as 4.683×10^{-9} (M) and 7.591×10^{-9} (M) for Zn^{2+} and Co^{2+} ions, respectively, using the equation:

$$\mathrm{DL} = K \times \frac{\sigma}{S}$$

where K = 2 or 3 (we take 3 in this case), σ is the standard deviation of the blank solution and S is the slope of the calibration

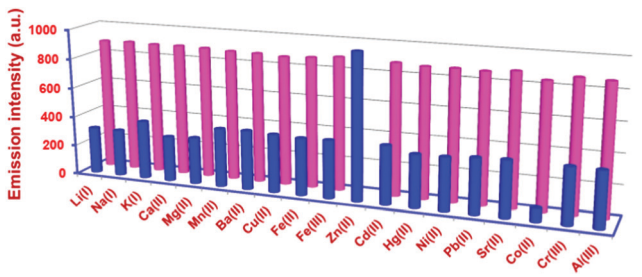

Fig. 4 Blue bars: variation of the fluorescence intensity of **Hmpye** (5×10^{-7} M) in the presence of 2 equiv. of various cations in HEPES buffer (pH = 7.4) solution. Pink bars: fluorescence intensity of a mixture of **Hmpye** (5×10^{-7} M) solution with other metal ions, followed by addition of Zn^{2+} to the solution (λ_{ex} = 340 nm, λ_{em} = 461 nm).

curve[28] (Fig. S9 and S10, ESI†). Furthermore, the association constants (K_a) of **Hmpye** for Zn^{2+} and Co^{2+} coordination were calculated for a 1 : 2 stoichiometry (host : guest) on the basis of the Benesi–Hildebrand plot and were found to be 5.203×10^{12} (M^{-2})

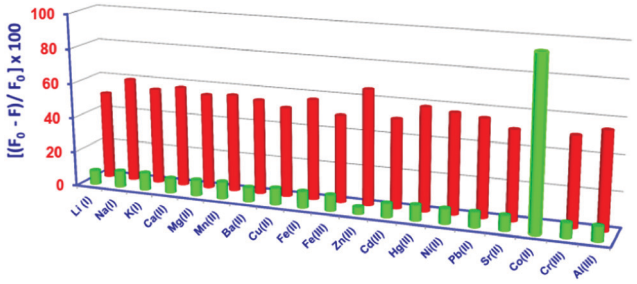

Fig. 5 Green bars: fluorescence quenching efficiency (FQE) of **Hmpye** (5×10^{-7} M) in the presence of 2 equiv. of various cations in HEPES buffer (pH = 7.4) solution. Red bars: fluorescence quenching efficiency (FQE) of a mixture of **Hmpye** (5×10^{-7} M) solution with other metal ions, followed by addition of Co^{2+} to the solution (λ_{ex} = 340 nm, λ_{em} = 503 nm).

and 9.783×10^{11} (M^{-2}), respectively[22d,29] (Fig. S11 and S12, ESI†). This preferential fluorescence enhancement for Zn^{2+} might be due to the formation of a chelate complex (rigid system) between **Hmpye** and Zn^{2+} ions, leading to the chelation-enhanced fluorescence (CHEF) effect. Upon stable chelation with Zn^{2+} ions, the C=N isomerization and excited-state intramolecular proton transfer (ESIPT) involving the phenolic OH from the 4-methylphenyl moiety might be inhibited, leading to a fluorescence enhancement[30] (Scheme 3).

To establish the reversibility of **Hmpye** towards Zn^{2+}/Co^{2+}, the reversibility experiment was carried out by sequentially adding Na_2EDTA/Zn^{2+} or Co^{2+} to a mixture of receptor **Hmpye** + Zn^{2+} and **Hmpye** + Co^{2+}, respectively (Fig. S13 and S14, ESI†). The successful outcome indicates that **Hmpye** can be reused with proper treatment and interesting for real-time applications to sense Zn^{2+}/Co^{2+}.

This quenching of the initial fluorescence intensity of **Hmpye** induced by Co^{2+} ions is attributed to the reverse photoinduced electron transfer (reverse PET) from the 4-methylphenyl moiety to the phenolic OH and imine nitrogen because of the decrease in the electron density upon Co^{2+} ion complexation[31] (Scheme S2, ESI†).

For practical applications, the effects of pH on the fluorescence intensity of **Hmpye** in the presence and absence of both

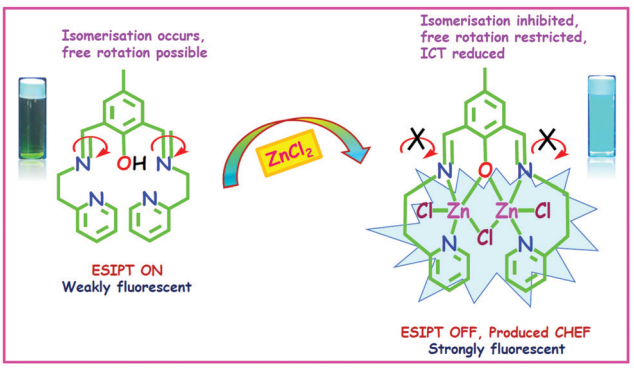

Scheme 3 Schematic illustration of the proposed mechanism for the fluorescence changes of the chemosensor (**Hmpye**) upon the addition of Zn^{2+}.

the metals (Zn^{2+}/Co^{2+}) were measured by adjusting the pH by HCl and NaOH (Fig. S15 and S16, ESI†). In the pH range of 5.0–9.0, an enhancement of fluorescence intensity was observed upon the addition of Zn^{2+} and the presence of Co^{2+}, and the quenched fluorescence was almost unaffected over a wide range, from pH 3.0 to 11.0. Hence, pH 7.4 was maintained throughout Zn^{2+} sensing studies as this value was closer to the physiological pH. Therefore, **Hmpye** can detect Zn^{2+} and Co^{2+} over a wide range of pH with a high selectivity and specificity.

The average fluorescence lifetime of **Hmpye** was measured in the presence and absence of Zn^{2+}/Co^{2+} ions in HEPES buffer (pH = 7.4) solution (Fig. S17 and S18, ESI†). According to the equations, $\tau^{-1} = k_r + k_{nr}$ and $k_r = \Phi_f/\tau$, the radiative decay rate constant k_r and the total nonradiative decay rate constant k_{nr} of **Hmpye**, Zn^{2+}-bound and Co^{2+}-bound species were found. The average lifetimes were calculated as 3.56 ns for **Hmpye** only, 4.89 ns for the mixture of **Hmpye** + Zn^{2+}, and 2.13 ns for **Hmpye** + Co^{2+} (Table S4, ESI†).

3.4. Application of Hmpye for Zn^{2+}/Co^{2+} detection in live cells

The probe **Hmpye** has a thermodynamically favourable binding affinity to $Zn(NO_3)_2{\cdot}6H_2O$ and both of these form a probe–$Zn(NO_3)_2{\cdot}6H_2O$ complex which gives an emission spectrum in the visible range. Keeping this in mind it was conceived that the compound could be exploited for fluorescence imaging of live cells, particularly for sensitive detection of intracellular zinc. However, to materialize this objective it is a prerequisite to assess the cytotoxic effect of the probe compound, $Zn(NO_3)_2{\cdot}6H_2O$ and their complex on live cells. The conventional MTT assay, which is based on the mitochondrial dehydrogenase activity of viable cells was adopted to study the cytotoxicity of the above-mentioned compounds at varying concentrations mentioned in the materials and physical methods section. Fig. S19 (ESI†) shows that the probe **Hmpye**, $Zn(NO_3)_2{\cdot}6H_2O$, $Co(NO_3)_2{\cdot}6H_2O$ and their respective complexes did not exert any adverse effect on cell viability at lower concentrations. However, exposure of HeLa cells to the probe–Zn^{2+}/Co^{2+} complex resulted in a decline in cell viability above a 30 μM concentration. The effect was more pronounced at higher concentrations and showed an adverse cytotoxic effect in a dose-dependent manner. The observed cytotoxic effect could be due to the high concentration of probe–salt complex formation which negatively affects cell survival. However, a lower concentration of probe/salt was not harmful to cells and thus can be used for *in vitro* live cell studies.

The results obtained in the *in vitro* cytotoxic assay suggested that, in order to pursue fluorescence imaging studies of the probe–zinc complex in live cells, a working concentration of 20 μM for the probe compound will be optimum. Hence, to assess the effectiveness of the compound as a probe for intracellular detection of Zn^{2+}/Co^{2+} by fluorescence microscopy, HCT cells were treated with 20 μM $Zn(NO_3)_2{\cdot}6H_2O$ for 30 min, followed by 10 μM probe solution, to promote formation of the **Hmpye**–Zn^{2+} complex. Fluorescence microscopy studies revealed no fluorescence in cells when treated with either **Hmpye** or $Zn(NO_3)_2{\cdot}6H_2O$ alone (Fig. 6, panels A and B) and $Co(NO_3)_2{\cdot}6H_2O$ alone (Fig. 7, panels A and B). Upon incubation

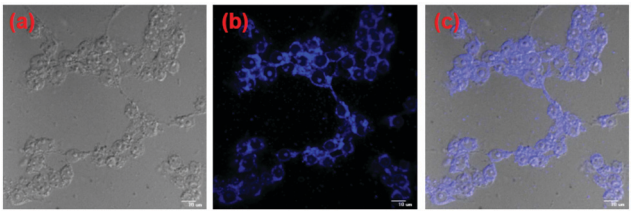

Fig. 6 Fluorescence confocal images of the probe **Hmpye** and $Zn(NO_3)_2{\cdot}6H_2O$ in HCT cells. All images were acquired with a 40× objective lens. (a) Bright field image of the cells without any treatment. (b) Cells treated with only zinc salt (20 μM), nuclei counterstained with DAPI (1 μg mL^{-1}). (c) Dark field image of the cells treated with $Zn(NO_3)_2{\cdot}6H_2O$ (20 μM), followed by **Hmpye** (20 μM), nuclei counterstained with DAPI (1 μg mL^{-1}).

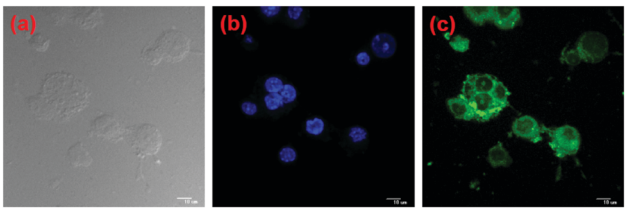

Fig. 7 Fluorescence confocal images of HCT cells treated with $Zn(NO_3)_2{\cdot}6H_2O$, followed by **Hmpye** and then $Co(NO_3)_2{\cdot}6H_2O$. All images were acquired with a 40× objective lens. (a) Bright field image of the cells without any treatment. (b) Cells treated with only cobalt salt (20 μM), nuclei counterstained with DAPI (1 μg mL^{-1}). (c) Dark field image of the cells treated with $Zn(NO_3)_2{\cdot}6H_2O$ (20 μM), followed by **Hmpye** (20 μM) and then $Co(NO_3)_2{\cdot}6H_2O$ (20 μM), nuclei counterstained with DAPI (1 μg mL^{-1}).

with $Zn(NO_3)_2{\cdot}6H_2O$, followed by the probe compound, a striking switch-on fluorescence was observed inside the cells (Fig. 6(c)) in the visible range (460–465 nm) which indicated the formation of the probe–zinc complex, as observed earlier in solution studies. An intense blue fluorescence was observed in the cytoplasmic region, strongly suggesting that the probe compound **Hmpye** could readily cross the membrane barrier, permeate into HCT cells, and rapidly sense intracellular Zn^{2+}. In a separate set of experiments as mentioned in the method section the cells were treated with Zn^{2+} salt, followed by **Hmpye,** and then incubated with Co^{2+} salt. When observed under a fluorescence microscope, the cells showed green emission. This is significant because due to the presence of Co^{2+} salt the zinc fluorescence was quenched and gave bright green emission of wavelengths in the range of 500 to 505 nm. It should be noted here that the bright field images of treated cells did not reveal any gross morphological changes, which suggested that the cells were viable. These findings open up the avenue for future *in vivo* applications of the chemosensor to detect Zn^{2+} and Co^{2+}.

4. Conclusions

Herein, the effectiveness of a diformyl phenol based chemosensor, 4-methyl-2,6-bis-[(2-pyridin-2-yl-ethylimino)-methyl]-phenol (**Hmpye**), for selective nanomolar detection of Zn^{2+} and Co^{2+} in 100% aqueous solution has been demonstrated. The probe structure contains suitably positioned phenolic OH and imine groups which are capable of participating in the ESIPT process. The selectivity of **Hmpye** towards Zn^{2+} and Co^{2+} has been extensively studied by means of absorption and emission spectral experiments. **Hmpye** can sense Zn^{2+} by means of selective fluorescence enhancement at 461 nm, whereas Co^{2+} quenches the fluorescence of **Hmpye** at 503 nm. Absorption-fluorescence titration profiles have been investigated to reveal the intricate interactions of the probe and the analytes. Job's plot points out that the sensing phenomenon has been driven by a 1 : 2 Hmpye : analyte complex formation. ESI-MS experimental outcomes clearly affirm the above-mentioned ratio. Moreover, we have been able to obtain the single crystal structure of the Hmpye : Zn^{2+} complex, $[Zn_2(mpye)(Cl)_3]$, which confirms the composition of the ensemble and the binding mode. The outcome of competitive studies and reversible sensing behavior add further effectiveness to **Hmpye**. Furthermore, the utility of **Hmpye** has also been examined in HCT live cells which displayed positive outcomes.

Conflicts of interest

There are no conflicts to declare.

Acknowledgements

B. Naskar acknowledges the University Grants Commission, India for fellowship (sanction no. RGNF-2013-14-SC-WES-38844). The Department of Chemistry, DST-FIST, DST-PURSE, and CAS(V) are gratefully acknowledged for providing the X-ray diffraction and HRMS facilities.

Notes and references

1 (*a*) D. Udhayakumari and V. Inbaraj, *J. Fluoresc.*, 2020, **30**, 1203–1223; (*b*) S. Khan, X. Chen, A. Almahri, E. S. Allehyani, F. A. Alhumaydhi, M. M. Ibrahim and S. Ali, *J. Environ. Chem. Eng.*, 2021, **9**, 106381; (*c*) P. Roy, *Coord. Chem. Rev.*, 2021, **427**, 213562; (*d*) P. Roy, K. Dhara, M. Manassero and P. Banerjee, *Inorg. Chim. Acta*, 2009, **362**, 2927–2932; (*e*) S. Dey, A. Roy, G. P. Maiti, S. K. Mandal, P. Banerjee and P. Roy, *New J. Chem.*, 2016, **40**, 1365–1376; (*f*) S. Alamgir, M. M. Rhaman, I. Basaran, D. R. Powell and M. A. Hossain, *Polyhedron*, 2020, **187**, 114681; (*g*) M. Kumar, A. Kumar, M. K. Singh, S. K. Sahu and R. P. John, *Sens. Actuators, B*, 2017, **241**, 1218–1223; (*h*) M. Hosseinia, Z. Vaezi, M. R. Ganjali, F. Faridbod, S. D. Abkenar, K. Alizadeh and M. Salavati-Niasari, *Spectrochim. Acta, Part A*, 2010, **75**, 978–982; (*i*) J. Yan, L. Fan, J. Qin, C. Li and Z. Yang, *Tetrahedron Lett.*, 2016, **57**, 2910–2914; (*j*) A. Roy, M. Nandi and P. Roy, *TrAC, Trends Anal. Chem.*, 2021, **138**, 116204.

2 (*a*) M. Patil, S. Bothra, S. K. Sahoo, H. A. Rather, R. Vasita, R. Bendre and A. Kuwar, *Sens. Actuators, B*, 2018, **270**, 200–206; (*b*) L. Ma, G. Liu, S. Pu, C. Zheng and C. Fan,

Tetrahedron, 2017, **73**, 1691–1697; (*c*) C. Andreini and I. Bertini, *J. Inorg. Biochem.*, 2012, **111**, 150–156; (*d*) E. Kimura, S. Aoki, E. Kikuta and T. Koike, *Proc. Natl. Acad. Sci. U. S. A.*, 2003, **100**, 3731–3736; (*e*) M. Cassandri, A. Smirnov, F. Novelli, C. Pitolli, M. Agostini, M. Malewicz, G. Melino and G. Raschellà, *Cell Death Discovery*, 2017, **3**, 17071.

3 (*a*) J. H. Weiss, S. L. Sensi and J. Y. Koh, *Trends Pharmacol. Sci.*, 2000, **21**, 395–401; (*b*) S. Y. Assaf and S. H. Chung, *Nature*, 1984, **308**, 734–736; (*c*) S. Yamasaki, A. Hasegawa, S. Hojyo, W. Ohashi, T. Fukada, K. Nishida and T. Hirano, *PLoS One*, 2012, **7**, e39654; (*d*) Y. V. Li, *Endocrine*, 2014, **45**, 178–189; (*e*) C. J. Frederickson, J.-Y. Koh and A. I. Bush, *Nat. Rev. Neurosci.*, 2005, **6**, 449–462.

4 (*a*) M. Gutiérrez, K. Mickus and L. M. Camacho, *Sci. Total Environ*, 2016, **565**, 392–400; (*b*) J. Wu, J. Long, L. Liu, J. Li, H. Liao, M. Zhang, C. Zhao and Q. Wu, *Int. J. Environ. Res. Public Health*, 2018, **15**, 1838; (*c*) A. B. Chausmer, *J. Am. Coll. Nutr.*, 1998, **17**, 109–115; (*d*) K. Hirzel, U. Muller, A. T. Lata, S. Hülsmann, J. Grudzinska, M. W. Seeliger, H. Betz and B. Laube, *Neuron*, 2006, **52**, 679–690; (*e*) Z. Xu, K.-H. Baek, H. N. Kim, J. Cui, X. Qian, D. R. Spring, I. Shin and J. Yoon, *J. Am. Chem. Soc.*, 2010, **132**, 601–610; (*f*) S. K. Ghosh, P. Kim, X. A. Zhang, S. H. Yun, A. Moore, S. J. Lippard and Z. Medarova, *Cancer Res.*, 2010, **70**, 6119–6127.

5 Q. Li, X. H. Zhao, Q. Z. Lv and G. G. Liu, *Sep. Purif. Technol.*, 2007, **55**, 76–81.

6 (*a*) Y. Liu, P. Liang and L. Guo, *Talanta*, 2005, **68**, 25–30; (*b*) *Inductively Coupled Plasma Mass Spectrometry*, ed. A. Montaser, Wiley-VCH, New York, 1998.

7 A. A. Ensafi, T. Khayamian and A. Benvidi, *Anal. Chim. Acta*, 2006, **561**, 225–232.

8 M. Kumar, A. Kumar, M. S.-H. Faizi, S. Kumar, M. K. Singh, S. K. Sahu, S. Kishor and R. P. John, *Sens. Actuators, B*, 2018, **260**, 888–899.

9 (*a*) G. A. Knauer, J. H. Martin and R. M. Gordon, *Nature*, 1982, **297**, 49–51; (*b*) P. J. Santander, Y. Kajiwara, H. J. Williams and A. I. Scott, *Bioorg. Med. Chem.*, 2006, **14**, 724–731; (*c*) R. A. Colvin, A. I. Bush, I. Volitakis, C. P. Fontaine, D. Thomas, K. Kikuchi and W. R. Holmes, *Am. J. Physiol.: Cell Physiol.*, 2008, **294**, C726–C742; (*d*) A. Krężel and W. Maret, *J. Biol. Inorg. Chem.*, 2006, **11**, 1049–1062; (*e*) L. A. Gaither and D. J. Eide, *Biometals*, 2001, **14**, 251–270; (*f*) D. J. Eide, *Biochim. Biophys. Acta.*, 2006, **1763**, 711–722.

10 (*a*) A. Frank, J. McPartlin and R. Danielsson, *Sci. Total Environ.*, 2004, **318**, 89–100; (*b*) K. Al-Habsi, E. H. Johnson, I. T. Kadim, A. Srikandakumar, K. Annamalai, R. Al-Busaidy and O. Mahgoub, *Vet. J.*, 2007, **173**, 133–139; (*c*) C.-Y. Tsai and Y. Lin, *Analyst.*, 2013, **138**, 1232–1238; (*d*) C. Li, X. Zhang, Z. Jin, R. Han, G. Shen and R. Yu, *Anal. Chim. Acta.*, 2006, **580**, 143–148; (*e*) D. Maity and T. Govindaraju, *Inorg. Chem.*, 2011, **50**, 11282–11284; (*f*) D. Ou, L. Zhang, Y. Huang, X. Lou, J. Qin and Z. Li, *Macromol. Rapid Commun.*, 2013, **34**, 759–766; (*g*) Y. Leng, F. Zhang, Y. Zhang, X. Fu, Y. Weng, L. Chen and A. Wu, *Talanta*, 2012, **94**, 271–277; (*h*) S. H. Mashraqui, M. Chandiramani, R. Betkar and K. Poonia, *Tetrahedron Lett.*, 2010, **51**, 1306–1308; (*i*) X. Wang, W. Zheng, H. Lin, G. Liu, Y. Chen and J. Fang, *Tetrahedron Lett.*, 2009, **50**, 1536–1538.

11 (*a*) O. R. Crick and F. D. Othmer, *Encyclopedia of Chemical Technology*, Wiley, 1982, vol. 5, p. 851; (*b*) A. Leonard and R. Lauwerys, *Mutat. Res.*, 1990, **239**, 17–27; (*c*) A. I. Seldén, C. Norberg, C. K. Stiber and E. H. Lindberg, *Environ. Toxicol. Pharmacol.*, 2007, **23**, 129–131; (*d*) M. Jullig, X. Y. Chen, A. J. Hickey, D. J. Crossman, A. M. Xu, Y. Wang, D. R. Greenwood, Y. S. Choong, S. J. Schonberger, M. J. Middleditch, A. R.-J. Phillips and G. J.-S. Cooper, *Proteomics: Clin. Appl.*, 2007, **1**, 387–399.

12 C. Reimann, F. Koller, G. Kashulina, H. Niskavaara and P. Englmaier, *Environ. Pollut.*, 2001, **115**, 239–252.

13 S. A. El-Safty, *Adsorption*, 2009, **15**, 227–239.

14 (*a*) E. Patel, C. Lynch, V. Ruff and M. Reynolds, *Toxicol. Appl. Pharmacol.*, 2012, **258**, 367–375; (*b*) D. C. Barceloux, *Clin. Toxicol.*, 1999, **37**, 201–208; (*c*) D. Maity, V. Kumar and T. Govindaraju, *Org. Lett.*, 2012, **14**, 6008–6011; (*d*) C. Y. Li, X. B. Znang, Z. Jin, R. Hari, G. L. Shen and R. Q. Yu, *Anal. Chim. Acta*, 2006, **580**, 143–148; (*e*) D. Maity, A. Raj, D. Karthigeyan, T. K. Kundu and T. Govindaraju, *RSC Adv.*, 2013, **3**, 16788–16794.

15 (*a*) M. Gharehbaghi, F. Shemirani and M. D. Farahani, *J. Hazard. Mater.*, 2009, **165**, 1049–1055; (*b*) A. R. Khorrami, T. Hashempur, A. Mahmoudi and A. R. Karimi, *Microchem. J.*, 2006, **84**, 75–79.

16 O. Karovic, I. Tonazzini, N. Rebola, E. Edström, C. Lövdahl, B. B. Fredholm and E. Dare, *Biochem. Pharmacol.*, 2007, **73**, 694–708.

17 (*a*) F. Monteil-Rivera and J. Dumonceau, *Anal. Bioanal. Chem.*, 2002, **374**, 1105–1112; (*b*) W. Y. Lin, L. Yuan, L. L. Long, C. C. Guo and J. B. Feng, *Adv. Funct. Mater.*, 2008, **18**, 2366–2372; (*c*) D. Maity and T. Govindaraju, *Inorg. Chem.*, 2011, **50**, 11282–11284; (*d*) Y. Yao, D. Tian and H. Li, *ACS Appl. Mater. Interfaces*, 2010, **2**, 684–690; (*e*) S. J. Zhen, F. L. Guo, L. Q. Chen, Y. F. Li, Q. Zhang and C. Z. Huang, *Chem. Commun.*, 2011, **47**, 2562–2564; (*f*) H. Y. Au-Yeung, E. J. New and J. C. Chang, *Chem. Commun.*, 2012, **48**, 5268–5270.

18 (*a*) In *Inductively Coupled Plasma Emission Spectrometry*, ed. P. W. J. M. Boumans, Wiley, New York, 1987; (*b*) Y. Xu, J. Zhou, G. Wang, J. Zhou and G. Tao, *Anal. Chim. Acta*, 2007, **584**, 204–209; (*c*) L. Zhao, S. Zhong, K. Fang, Z. Qian and J. Chen, *J. Hazard. Mater.*, 2012, **239-240**, 206–212; (*d*) K. S. Rao, T. Balaji, T. PrasadaRao, Y. Babu and G. R.-K. Naidu, *Spectrochim. Acta, Part B*, 2002, **57**, 1333–1338; (*e*) G. Collado Gomez, A. Garcia de Torres, J. M. Cano Pavon and C. Bosch Ojeda, *Anal. Lett.*, 1995, **28**, 1181–1196; (*f*) A. R. Khorrami, T. Hashempur, A. Mahmoudi and A. R. Karimi, *Microchem. J.*, 2006, **84**, 75–79; (*g*) A. R. Khorrami, A. R. Fakhari, M. Shamsipur and H. Naeimi, *Environ. Anal. Chem.*, 2009, **89**, 319–329.

19 M. Ghaedi, F. Ahmadi and A. Shokrollahi, *J. Hazard. Mater.*, 2007, **142**, 272–278.

20 (*a*) Z. Gao, G. Wang, P. Li and Z. Zhao, *Anal. Chem.*, 1991, **63**, 953–957; (*b*) M. Morfobos, A. Economou and A. Voulgaropoulos, *Anal. Chim. Acta*, 2004, **519**, 57–64; (*c*) A. Bottcher, T. Takeuchi, K. I. Hardcastle, T. J. Meade and H. B. Gray, *Inorg. Chem.*, 1997, **36**, 2498–2504.

21 (*a*) K. B. Kim, H. Kim, E. J. Song, S. Kim, I. Noh and C. Kim, *Dalton Trans.*, 2013, **42**, 16569–16577; (*b*) J. Wang, B. Liu, X. Liu, M. J. Panzner, C. Wesdemiotis and Y. Pang, *Dalton Trans.*, 2014, **43**, 14142–14146; (*c*) J. Wang, Y. Li, E. Duah, S. Paruchuri, D. Zhou and Y. Pang, *J. Mater. Chem. B.*, 2014, **2**, 2008–2012; (*d*) A. J. Sanchez, B. Ortiz, V. O. Navarrete, N. Farfan and R. Santillan, *Analyst.*, 2015, **140**, 6031–6039; (*e*) H. N. Kim, Z. Q. Guo, W. H. Zhu, J. Yoon and H. Tian, *Chem. Soc. Rev.*, 2011, **40**, 79–93; (*f*) A. Razgulin, N. Ma and J. H. Rao, *Chem. Soc. Rev.*, 2011, **40**, 4186–4216; (*g*) J. Chan, S. C. Dodani and C. J. Chang, *Nat. Chem.*, 2012, **4**, 973–984; (*h*) P. A. Gale, S. E. Garcia-Garrido and J. Garric, *Chem. Soc. Rev.*, 2008, **37**, 151–190; (*i*) M. Formica, V. Fusi, L. Giorgi and M. Micheloni, *Coord. Chem. Rev.*, 2012, **256**, 170–192; (*j*) Y. Zhou, Z. Xu and J. Yoon, *Chem. Soc. Rev.*, 2011, **40**, 2222–2235; (*k*) X. Chen, Y. Zhou, X. Peng and J. Yoon, *Chem. Soc. Rev.*, 2010, **39**, 2120–2135; (*l*) J. F. Zhang, Y. Zhou, J. Yoon and J. S. Kim, *Chem. Soc. Rev.*, 2011, **40**, 3416–3429; (*m*) H. Kobayashi, M. Ogawa, R. Alford, P. L. Choyke and Y. Urano, *Chem. Rev.*, 2010, **110**, 2620–2640; (*n*) J. F. Callan, A. P. de Silva and D. C. Magri, *Tetrahedron*, 2005, **61**, 8551–8588; (*o*) A. P. Demchenko, *Introduction to Fluorescence Sensing*, Springer, New York, 2008; (*p*) R. Y. Tsien, in *Fluorescent and Photochemical Probes of Dynamic Biochemical Signals inside Living Cells*, ed. A. W. Czarnik, American Chemical Society, Washington, DC, 1993, pp. 130–146; (*q*) Y. Xiang, A. J. Tong, P. Y. Jin and Y. Ju, *Org. Lett.*, 2006, **8**, 2863–2866.

22 (*a*) B. Naskar, R. Modak, Y. Sikdar, D. K. Maiti, A. Banik, T. K. Dangar, S. Mukhopadhyay, D. Mandal and S. Goswami, *J. Photochem. Photobiol., A.*, 2016, **321**, 99–109; (*b*) B. Naskar, R. Modak, D. K. Maiti, S. K. Mandal, J. K. Biswas, T. K. Mondal and S. Goswami, *Polyhedron*, 2016, **117**, 834–846; (*c*) B. Naskar, R. Modak, Y. Sikdar, D. K. Maiti, A. Bauzá, A. Frontera, A. Katarkar, K. Chaudhuri and S. Goswami, *Sens. Actuators, B*, 2017, **239**, 1194–1204; (*d*) B. Naskar, R. Modak, D. K. Maiti, A. Bauzá, A. Frontera, P. K. Maiti, S. Mandal and S. Goswami, *RSC Adv.*, 2017, **7**, 11312–11321; (*e*) B. Naskar, A. Dhara, R. Modak, D. K. Maiti, C. Prodhan, K. Chaudhuri, A. Requena, J. P.-C. Carrasco and S. Goswami, *ChemistrySelect*, 2017, **2**, 2512–2519; (*f*) S. Chakraborty, C. R. Bhattacharjee, P. Mondal, S. K. Prasad and D. S.-S. Rao, *Dalton Trans.*, 2015, **44**, 7477–7488; (*g*) K. Li and A. Tong, *Sens. Actuators, B*, 2013, **184**, 248–253; (*h*) F. U. Rahman, A. Ali, R. Guoa, J. Tiana, H. Wanga, Z. T. Lia and D. W. Zhang, *Sens. Actuators, B*, 2015, **211**, 544–550; (*i*) V. K. Gupta, A. K. Singh, L. K. Kumawat and N. Mergu, *Sens. Actuators, B*, 2016, **222**, 468–482; (*j*) D. Buccella, J. A. Horowitz and S. J. Lippard, *J. Am. Chem. Soc.*, 2011, **133**, 4101–4114; (*k*) K. Komatsu, Y. Urano, H. Kojima and T. Nagano, *J. Am. Chem. Soc.*, 2007, **129**, 13447–13454; (*l*) P. Du and S. J. Lippard, *Inorg. Chem.*, 2010, **49**, 10753–10755; (*m*) E. Tomat and S. J. Lippard, *Inorg. Chem.*, 2010, **49**, 9113–9115; (*n*) B. A. Wong, S. Friedle and S. J. Lippard, *Inorg. Chem.*, 2009, **48**, 7009–7011.

23 (*a*) M. Sohrabi, M. Amirnasr, S. Meghdadi, M. Lutz, M. B. Torbati and H. Farrokhpour, *New J. Chem.*, 2018, **42**, 12595–12606; (*b*) G. Singh, S. Priyanka, S. Diksha, J. D. Kaur, A. Saini, A. Devi and P. Satija, *Inorg. Chim. Acta*, 2021, **525**, 120465; (*c*) G. Jin, J. Jun, G. Rim, L. Nguyen, I. Noh and C. Kim, *Sens. Actuators, B*, 2016, **223**, 509–519; (*d*) S. Y. Lee, S. Y. Kim, J. A. Kim and C. Kim, *J. Lumin.*, 2016, **179**, 602–609; (*e*) R. Purkait, A. D. Mahapatra, D. Chattopadhyay and C. Sinha, *Spectrochim. Acta, Part A*, 2019, **207**, 164–172; (*f*) U. C. Saha, B. Chattopadhyay, K. Dhara, S. K. Mandal, S. Sarkar, A. R. KhudaBukhsh, M. Mukherjee, M. Helliwell and P. Chattopadhya, *Inorg. Chem.*, 2011, **50**, 1213–1219; (*g*) K. Mawai, S. Nathani, P. Roy, U. P. Singh and K. Ghosh, *Dalton Trans.*, 2018, **47**, 6421–6434; (*h*) T. A. Khan, M. Sheoran, M. V.-N. Raj, S. Jain, D. Gupta and S. G. Naik, *Spectrochim. Acta, Part A*, 2018, **189**, 176–182; (*i*) S. Lohar, S. Pal, M. Mukherjee, A. Maji, N. Demitri and P. Chattopadhyay, *RSC Adv.*, 2017, **7**, 25528–25534; (*j*) A. Jana, B. Das, S. K. Mandal, S. Mabhai, A. R. KhudaBukhsh and S. Dey, *New J. Chem.*, 2016, **40**, 5976–5984; (*k*) A. Jana, P. K. Sukul, S. K. Mandal, S. Konar, S. Ray, K. Das, J. A. Golen, A. L. Rheingold, S. Mondal, T. K. Mondal, A. R. Khuda-Bukhsh and S. K. Kar, *Analyst*, 2014, **139**, 495–504; (*l*) T. Mistri, M. Dolai, D. Chakraborty, A. R. Khuda-Bukhsh, K. K. Das and M. Ali, *Org. Biomol. Chem.*, 2012, **10**, 2380–2384; (*m*) P. Roy, K. Dhara, M. Manassero, J. Ratha and P. Banerjee, *Inorg. Chem.*, 2007, **46**, 6405–6412; (*n*) K. Sarkar, K. Dhara, M. Nandi, P. Roy, A. Bhaumik and P. Banerjee, *Adv. Funct. Mater.*, 2009, **19**, 223–234; (*o*) J. M. Jung, S. Y. Lee, E. Nam, M. H. Lim and C. Kim, *Sens. Actuators, B*, 2017, **244**, 1045–1053; (*p*) H. Liu, Y. Dong, B. Zhang, F. Liu, C. Tan, Y. Tan and Y. Jiang, *Sens. Actuators, B*, 2016, **234**, 616–624; (*q*) Y. J. Na, Y. W. Choi, G. R. You and C. Kim, *Sens. Actuators, B*, 2016, **223**, 234–240; (*r*) D. Vashisht, K. Kaur, R. Jukaria, A. Vashisht, S. Sharma and S. K. Mehta, *Sens. Actuators, B*, 2019, **280**, 219–226; (*s*) Y.-L. Liu, L. Yang, L. Li, Y.-Q. Guo, X.-X. Pang, P. Li, F. Ye and Y. Fu, *Molecules*, 2019, **24**, 3093; (*t*) L. Wang, X. Gong and Q. J. Bing, *Microchem. J.*, 2018, **142**, 279–287; (*u*) Z. D. Liu, W. L. Wang, H. J. Xu, L. Q. Sheng, S. S. Chen, D. Q. Huang and F. Sun, *Inorg. Chem. Commun.*, 2015, **62**, 19–23; (*v*) K. Y. Ryu, S. Y. Lee, D. Y. Park, S. Y. Kim and C. Kim, *Sens. Actuators, B*, 2016, **242**, 792–800; (*w*) J. M. Jung, S. Y. Lee and C. Kim, *Sens. Actuators, B*, 2017, **251**, 291–301; (*x*) S. Y. Lee, J. J. Lee, K. H. Bok, S. Y. Kim and C. Kim, *RSC Adv.*, 2016, **6**, 28081–28088; (*y*) K. Liu, P. Guo, L. J. Liu and X. F. Shi, *Sens. Actuators, B*, 2017, **250**, 667–672.

24 (*a*) R. R. Gagne, C. L. Spiro, T. J. Smith, C. A. Hamann, W. R. Thies and A. K. Shiemke, *J. Am. Chem. Soc.*, 1981, **103**, 4073–4081; (*b*) A. Guha, T. Chattopadhyay, N. D. Paul, M. Mukherjee, S. Goswami, T. Kumar Mondal, E. Zangrando and D. Das, *Inorg. Chem.*, 2012, **51**, 8750–8759.

25 G. M. Sheldrick, *SHELXL–97, Crystal Structure Refinement Program*, University of Göttingen, 1997.
26 K. Brandenburg, *Diamond, version 3.1e*, Crystal Impact GbR, Bonn, Germany, 2005.
27 A. W. Addison, T. N. Rao, J. Reedijk, J.-v Rijn and G. C. Verschoor, *J. Chem. Soc., Dalton Trans.*, 1984, 1349–1356.
28 (*a*) Y. P. Kumar, P. King and V. S.-K. R. Prasad, *Chem. Eng. J.*, 2006, **124**, 63–70; (*b*) M. Shortreed, R. Kopelman, M. Kuhn and B. Hoyland, *Anal. Chem.*, 1996, **68**, 1414–1418; (*c*) A. Caballero, R. Martíinez, V. Lloveras, I. Ratera, J. Vidal-Gancedo, K. Wurst, A. T′arraga, P. Molina and J. Veciana, *J. Am. Chem. Soc.*, 2005, **127**, 15666–15667; (*d*) W. Y. Lin, L. Yuan, Z. M. Cao, Y. M. Feng and L. Long, *Chem. – Eur. J.*, 2009, **15**, 5096–5103; (*e*) L. Rosa-Romo, M. T. Oropeza-Guzman, A. Olivas-Sarabia and G. Pina-Luis, *Sens. Actuators, B*, 2016, **233**, 459–468; (*f*) Q. Wu and E. V. Anslyn, *J. Am. Chem. Soc.*, 2004, **126**, 14682–14683; (*g*) T. Gunnlaugsson, J. P. Leonard and N. S. Murray, *Org. Lett.*, 2004, **6**, 1557–1560; (*h*) H. Qin, J. Ren, J. Wang and E. Wang, *Chem. Commun.*, 2010, **46**, 7385–7387.
29 (*a*) H. A. Benesi and J. H. Hildebrand, *J. Am. Chem. Soc.*, 1949, **71**, 2703–2707; (*b*) B. Naskar, R. Modak, D. K. Maiti, M. G.-B. Drew, A. Bauzá, A. Frontera, C. D. Mukhopadhyay, S. Mishra, K. D. Saha and S. Goswami, *Dalton Trans.*, 2017, **46**, 9498–9510; (*c*) H. Lineweaver and D. Burk, *J. Am. Chem. Soc.*, 1934, **56**, 658–666.
30 (*a*) A. Gupta and N. Kumar, *RSC Adv.*, 2016, **6**, 106413; (*b*) B. Naskar, D. K. Maiti, A. Bauzá, A. Frontera, C. Prodhan, K. Chaudhuri and S. Goswami, *ChemistrySelect*, 2017, **2**, 5414–5420; (*c*) H. Lu, W. Wang, X. Tan, X. Luo, M. Zhang, M. Zhang and S. Zang, *Dalton Trans.*, 2016, **45**, 8174–8181.
31 (*a*) S. Anbu, R. Ravishankaran, M. Fatima, C. Guedes da Silva, A. A. Karande and A. J.-L. Pombeiro, *Inorg. Chem.*, 2014, **53**, 6655–6664; (*b*) V. Chandrasekhar, S. Das, R. Yadav, S. Hossain, R. Parihar, G. Subramaniam and P. Sen, *Inorg. Chem.*, 2012, **51**, 8664–8666; (*c*) M. Kumar, R. Kumar, V. Bhalla, P. R. Sharma, T. Kaur and Y. Qurishi, *Dalton Trans.*, 2012, **41**, 408–412.